SCIENCE CHINA
Physics, Mechanics & Astronomy

•Letter to the Editor•

October 2019 Vol. 62 No. 10: 107421
https://doi.org/10.1007/s11433-019-9436-6

Orbital selection of the double [CuO_2] layer compound $Ca_3Cu_2O_4Cl_2$

JianFa Zhao[1,2], LiPeng Cao[1], WenMin Li[1,2], Jun Zhang[1,2], GuangYang Dai[1,2], Shuang Yu[1,2], QingQing Liu[1], XianCheng Wang[1], GuoQiang Zhao[1,2], YaTing Jia[1,2], Lei Duan[1,2], YouWen Long[1,2,3], Hong-Ji Lin[4], Chien-Te Chen[4], Liu-Hao Tjeng[5], ZhiWei Hu[5], RunZe Yu[1*], and ChangQing Jin[1,2,3*]

[1] *Institute of Physics, Chinese Academy of Sciences, Beijing 100190, China;*
[2] *School of Physics, University of Chinese Academy of Sciences, Beijing 100049, China;*
[3] *Songshan Lake Materials Laboratory, Dongguan 523808, China;*
[4] *Synchrotron Radiation Research Center, Hsinchu 30076, China;*
[5] *Max-Planck Institute for Chemical Physics of Solids, Dresden 01187, Germany*

Received May 17, 2019; accepted May 27, 2019; published online June 24, 2019

Citation: J. F. Zhao, L. P. Cao, W. M. Li, J. Zhang, G. Y. Dai, S. Yu, Q. Q. Liu, X. C. Wang, G. Q. Zhao, Y. T. Jia, L. Duan, Y. W. Long, H.-J. Lin, C.-T. Chen, L.-H. Tjeng, Z. W. Hu, R. Z. Yu, and C. Q. Jin, Orbital selection of the double [CuO_2] layer compound $Ca_3Cu_2O_4Cl_2$, Sci. China-Phys. Mech. Astron. **62**, 107421 (2019), https://doi.org/10.1007/s11433-019-9436-6

The discovery of high-temperature copper oxide superconductors (HTS) by Bednorz and Müller [1] in 1986 opened up a new field of superconductivity. Since then, several different families of materials have been discovered with greatly increased superconducting critical temperature (T_c) [2]. Oxychloride cuprates, $Ca_{n+1}Cu_nO_{2n}Cl_2$, are one such type of parent compound of high T_c cuprate superconductors. There are two members in this family known so far that can exist at ambient pressure: $Ca_2CuO_2Cl_2$ (single [CuO_2] layer CCOC) and $Ca_3Cu_2O_4Cl_2$ (double [CuO_2] layer CCOC). Both are composed of a [CuO_2] plane with the apical oxygen replaced by chlorine atoms. The superconducting transition temperature is observed above 80 K in double-layer oxychloride cuprates, which is 20 K higher than the transition observed for its pure oxide counterpart [3,4]. Compared to other copper oxide superconductors, a remarkable feature and advantage of these materials, from a structural point of view, is that the [CuO_2] plane in $Ca_{n+1}Cu_nO_{2n}Cl_2$ becomes geometrically more two dimensional due to the longer interlayer distance along the *c*-axis caused by the larger ionic radius of Cl^- compared to O^{2-} and has a stable surface after cleavage [5]. The much better two-dimensional feature of oxychloride cuprates is very suitable to study quantum emergent phenomena of the two-dimensional [CuO_2] plane via surface-sensitive angle-resolved photoemission spectroscopy or scanning tunneling microscopy measurements [6]. Previous studies have primarily focused on single [CuO_2] layer systems and have revealed the full electronic spectrum across the Mott-Hubbard gap [6]. A recent study revealed multiple underlying Fermi surfaces and an isotropic energy gap in $Ca_2CuO_2Cl_2$ [7]. Generally speaking, double-layer compounds usually have a much higher $T_{c,max}$ than their single-layer counterparts within each family of cuprate superconductors and the same is true for the $Ca_{n+1}Cu_nO_{2n}Cl_2$ family [3]. A recent study found that the double-layer compound has a much smaller charge transfer gap size (Δ_{CT}) than its single-layer counterpart, indicating a clear anticorrelation between Δ_{CT} and $T_{c,max}$ [8]. Because $Ca_3Cu_2O_4Cl_2$ has a more significant two-dimensional property than

*Corresponding authors (RunZe Yu, email: yurz@iphy.ac.cn; ChangQing Jin, email: jin@iphy.ac.cn)

$Ca_2CuO_2Cl_2$ due to the large distance between its layers, it is a good candidate to study the superconductivity mechanism in cuprates.

HTS are prototypical strongly correlated electron systems wherein the electronic states close to the Fermi energy E_F are primarily due to the hybridization of the Cu 3d and O 2p orbitals. The copper ion in the undoped parent compound is +2 with a $3d^9$ configuration, resulting in one hole occupied in the Cu 3d orbital. In fact, the Cu 3d orbital splits into a higher energy level e_g orbital and a lower energy level t_{2g} orbital in the oxygen octahedral crystal field stretched along the *c*-axis [9-11]. The distribution of the holes in the e_g orbital is strongly anisotropic, which plays an important role in HTS [9-11].

In this paper, we report the growth of high-quality $Ca_3Cu_2O_4Cl_2$ single crystals and characterizations of their magnetic and electronic properties. The unoccupied electronic structure of $Ca_3Cu_2O_4Cl_2$ is studied using polarization-dependent X-ray absorption spectroscopy at the O *K*-edge and the Cu $L_{2,3}$-edge.

$Ca_3Cu_2O_4Cl_2$ single crystals were grown via a self-flux method in two steps. First, polycrystalline $Ca_3Cu_2O_4Cl_2$ samples were prepared using a conventional solid-state reaction method from high-purity raw materials, CaO (Alfa, 99.95% pure), $CuCl_2$ (Alfa, 99.995% pure), and CuO (Alfa, 99.995% pure). The powder mixture of CaO, $CuCl_2$ and CuO with a molar ratio of 3:1:1 was ground together in a glove box under an Ar atmosphere. Then, the mixed powder was heated to 800°C for 20 h with several intermediate grindings to obtain single-phase samples. The quality of these polycrystalline $Ca_3Cu_2O_4Cl_2$ samples was examined using powder X-ray diffraction (XRD). In the second step, the polycrystalline $Ca_3Cu_2O_4Cl_2$ samples were placed in an alumina crucible and heated to 1333 K at a rate of 180 K/h, maintained at 1333 K for 10 h, and cooled to 1173 K at a rate of 30 K/h. The furnace was shut off at 1173 K to allow the samples to cool rapidly to room temperature to avoid generating the $Ca_2CuO_2Cl_2$ phase. High-quality and large-size $Ca_3Cu_2O_4Cl_2$ single crystals were obtained after the above experimental procedure.

XRD along the *c*-axis of the $Ca_3Cu_2O_4Cl_2$ single crystals was measured using a Rigaku XRD apparatus with Cu K_α radiation. A piece of a $Ca_3Cu_2O_4Cl_2$ single crystal, after being cleaned by tape, was placed on a silicon wafer and diffraction data were collected in the angle (2θ) range from 5° to 80° with steps of 0.01°. The microtopography of the single crystal was measured using a scanning electron microscope (SEM). The temperature dependence of the DC magnetic susceptibility of the $Ca_3Cu_2O_4Cl_2$ single crystal was measured using a vibrating sample magnetometer. The electrical transport properties along the $[CuO_2]$ plane were measured using a Quantum Design physical properties measurement system with a standard four-probe method.

The O 1s and Cu 2p X-ray absorption spectra measurements were performed at the Dragon Beamline of the National Synchrotron Radiation Research Center in Taiwan. The crystals were cleaved *in situ* and the shiny flat *ab*-plane surfaces were exposed. The chamber pressure was maintained at 5×10^{-9} Torr. Incoming photons were set to have 99% linear polarization with 0.15-eV energy resolution for O and 0.35-eV energy resolution for Cu. The spectra were recorded using the fluorescence-yield-detection method. To study the anisotropic distribution of the holes at the Cu 3d and O 2p states in $Ca_3Cu_2O_4Cl_2$, two polarization geometries with incident angles to the surface normal of 0° and 60° were chosen. In the geometry of normal incidence, the electric field vector *E* of the incoming radiation lies in the $[CuO_2]$ plane; in this case, the angle θ between *E* and the $[CuO_2]$ plane is 0° ($E \perp c$, θ=0°). To change the polarization, the sample was rotated around the *a*-axis by 60°. In the case of $Ca_3Cu_2O_4Cl_2$, the spectra for the electric field vector *E* perpendicular to the $[CuO_2]$ plane ($E // c$, θ=90°) can be obtained from the measured data using the formula, $I_{60°} = \cos^2(60°)I_{0°} + \sin^2(60°)I_{90°}$, where $I_{0°}$ and $I_{60°}$ are the measured intensities with θ = 0° and 60°, respectively [12]. CuO and NiO single crystal were used as reference for Cu $L_{2,3}$-edge and O *K*-edge, respectively [13]. These references were measured simultaneously in a separate chamber to calibrate the photon energy. The spectra were normalized by the photon flux to have the same intensities in the region well above the threshold [12]. Self-absorption effects were taken into account according to a procedure described in ref. [12].

Figure 1 shows the crystal structure of $Ca_3Cu_2O_4Cl_2$. $Ca_3Cu_2O_4Cl_2$ crystallizes into a $La_2CaCu_2O_6$-type tetragonal structure with a Cu–O_4–Cl five-coordinated pyramidal ligand of four oxide ions in a square-planar configuration and a chlorine ion in the lone apical site. The Cu–O_4–Cl five-coordinated ligand in $Ca_3Cu_2O_4Cl_2$ is the same as those Cu1212 or YBCO123; however, the latter also contain a Cu–O chain [14,15]. Therefore, $Ca_3Cu_2O_4Cl_2$ is an ideal compound with a pure Cu–O_4–Cl five-coordinated pyramidal ligand. The key points involved in the crystal growth are to reduce the $Ca_3Cu_2O_4Cl_2$ volatilization in the dwell process and to prevent the formation of the $Ca_2CuO_2Cl_2$ phase in the cooling process. $Ca_3Cu_2O_4Cl_2$ is more easily cleaved than $Ca_2CuO_2Cl_2$ due to the large distance between the layers. Figure S1 (Supporting Information) shows the XRD pattern for a $Ca_3Cu_2O_4Cl_2$ single crystal with the incident X-ray along the *c*-axis. Only sharp peaks along [00l] could be observed without any diffraction peak from the $Ca_2CuO_2Cl_2$ single crystal. The inset shows an optical photograph of $Ca_3Cu_2O_4Cl_2$ single crystal. The $Ca_3Cu_2O_4Cl_2$ single crystals formed as thin and flexible platelets, with irregular shapes, and the size of single crystal was up to approximately 6 mm × 10 mm × 0.2 mm. Figure S2 (Supporting Information) shows an SEM image of $Ca_3Cu_2O_4Cl_2$ single crystal, which

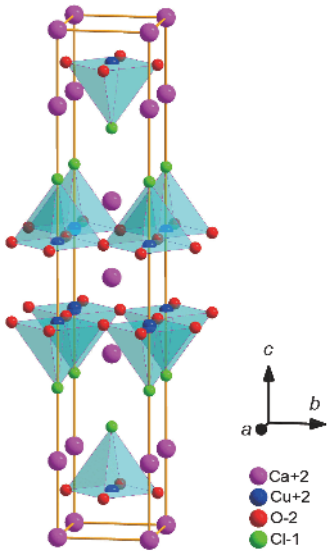

Figure 1 (Color online) The crystal structure of $Ca_3Cu_2O_4Cl_2$ with a double $[CuO_2]$ layer.

intuitively indicates that $Ca_3Cu_2O_4Cl_2$ is a layered quasi-two-dimensional material.

Figure 2(a) shows the temperature dependence of the magnetic susceptibility χ measured with external magnetic fields of 0.1 T perpendicular and parallel to *c*-axis. The magnetic susceptibility of the $Ca_3Cu_2O_4Cl_2$ single crystal shows strong anisotropy. The parent compounds of the high T_c cuprate superconductor are antiferromagnetic (AFM) insulators [4]. It is usually rather difficult to directly observe the AFM transition from magnetic susceptibility measurements [16]. However, looking at the magnetic susceptibility in the enlarged region shown in the inset of Figure 2(a), an obvious kink appears near 230 K. This can be defined as the Neel temperature of the AFM material [16]. Figure 2(b) shows the temperature dependence of the resistivity ρ for $Ca_3Cu_2O_4Cl_2$ single crystal in the $[CuO_2]$ plane. The resistivity increases with decreasing temperature, demonstrating a semiconducting behavior. The inset of Figure 2(b) shows the resistivity ρ from 160 K to 280 K. The resistivity changed singularly at 220-240 K, which is in agreement with the magnetic susceptibility measurement, revealing the AFM transformation in this temperature range.

Polarization-dependent soft X-ray absorption spectroscopy at the Cu $L_{2,3}$ and O *K*-edges is a powerful technique to explore the anisotropic distribution of the holes at the Cu 3d and O 2p states. Figure 3(a) shows the experimental geometry for the polarization-dependent X-ray absorption spectroscopy measurements. θ is the angle between the electric field vector E and the $[CuO_2]$ plane. Figure 3(b) shows a schematic diagram of d-orbital splitting in the crystal field with a Cu–O_6 six-coordinated octahedron ligand and a Cu–O_4–Cl five-coordinated pyramidal ligand. In O_h local symmetry, the 3d orbitals are split into the well-known

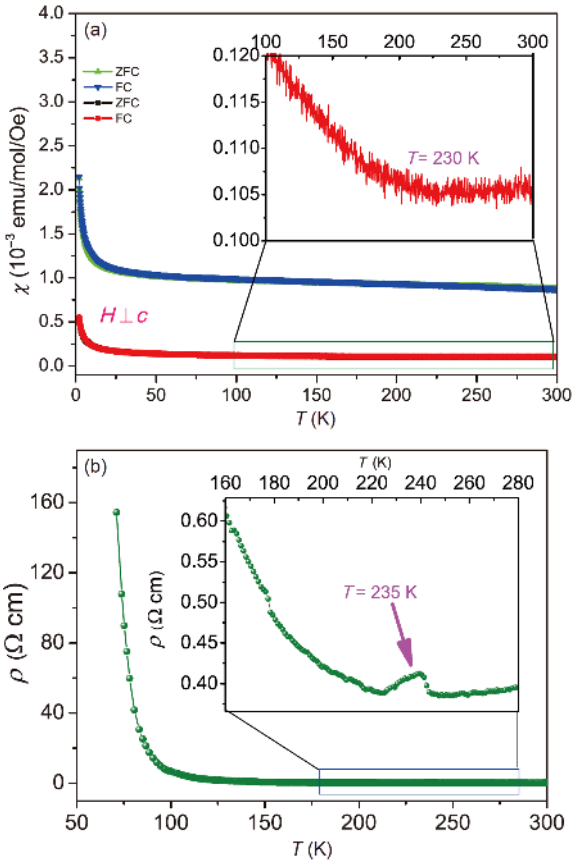

Figure 2 (Color online) (a) Temperature dependence of the DC magnetic susceptibility of a $Ca_3Cu_2O_4Cl_2$ single crystal with the external fields perpendicular and parallel to the *c*-axis. (b) The resistivity ρ as a function of the temperature for a $Ca_3Cu_2O_4Cl_2$ single crystal with a $[CuO_2]$ plane.

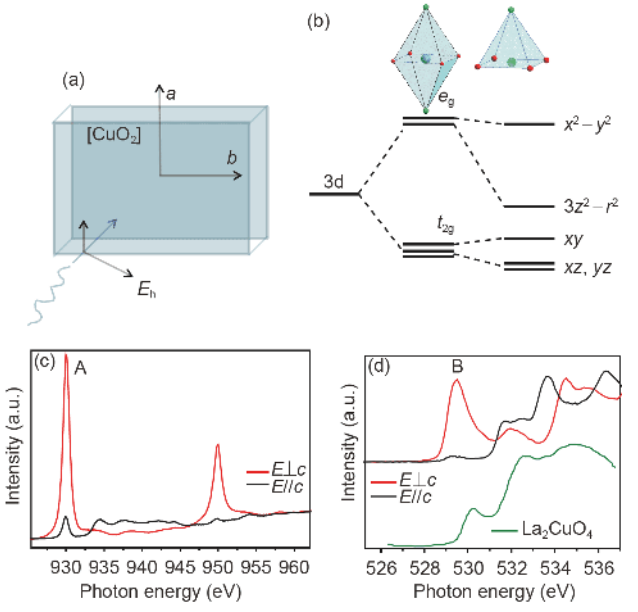

Figure 3 (Color online) (a) Experimental geometry for the polarization-dependent X-ray absorption spectroscopy measurements. (b) Schematic diagram of the *d*-level splitting of the Cu–O_4–Cl pyramidal ligand in $Ca_3Cu_2O_4Cl_2$. The polarization dependent, (c) Cu $L_{2,3}$-edge, and (d) O *K*-edge X-ray absorption spectra of $Ca_3Cu_2O_4Cl_2$ single crystals for different geometries.

e_g and t_{2g} suborbitals. For the five-coordinated pyramidal symmetry in the case of $Ca_3Cu_2O_4Cl_2$, the e_g orbitals are further split because the energy level of $3d_{z^2-r^2}$ becomes very low. Figure 3(c) presents the polarization-dependent Cu $L_{2,3}$-edge X-ray absorption spectra of the $Ca_3Cu_2O_4Cl_2$ single crystals for the $E\perp c$ and $E//c$ geometries. Peak A corresponds to the $3d^9\rightarrow Cu\underline{2p}_{3/2}3d^{10}$ transition, where $\underline{2p}_{3/2}$ denotes a Cu 2p core hole. The experimental spectrum shows a narrow peak at 931 eV, which is associated with the Cu 3d contributions to the upper Hubbard band (UHB). The spectral weights of peak A recorded in the $E\perp c$ geometry are much larger than those recorded in the $E//c$ geometry, showing that the Cu 3d contributions to the UHB are also primarily from the in-plane Cu $3d_{x^2-y^2}$ orbitals. Figure 3(d) shows the O *K*-edge X-ray absorption spectra of the $Ca_3Cu_2O_4Cl_2$ single crystals for the $E\perp c$ and $E//c$ geometries. Peak B is associated with the UHB and results from the $3d^{10}\underline{L}\rightarrow O\underline{1s}3d^{10}$ transition. Here $\underline{L}$ and $\underline{1s}$ denote the O $2p_{x,y}$ ligand hole and the O 1s core hole, respectively. The intensity of peak B primarily depends on the hybridization of the Cu 3d and O 2p orbitals. The anisotropy between the $E\perp c$ and $E//c$ geometries reveals that UHB is predominantly from the in-plane O $2p_x$ and O $2p_y$ orbitals. These results are similar to $(La_{2-x}Sr_x)CuO_4$ or $Sr_2CuO_2Cl_2$ with a "214" structure [10,17]. The distribution of the holes in the e_g orbital is strongly anisotropic, and nearly all of the holes occupied the in-plane Cu $3d_{x^2-y^2}$, O $2p_x$, and O $2p_y$ orbitals in $Ca_3Cu_2O_4Cl_2$. For comparison, the O *K*-edge XAS spectrum of the La_2CuO_4 compound taken from ref. [18] is also shown in Figure 3(d). One can see that UHB in $Ca_3Cu_2O_4Cl_2$ is a very dominant and well-resolved spectral feature compared to that in La_2CuO_4, where the UHB is a weak lower energy shoulder and its energy position is close to the absorption edge. Therefore, $Ca_3Cu_2O_4Cl_2$ is a suitable material to study the evolution of UHB with changing doping level.

High-quality single crystals of copper oxychloride $Ca_3Cu_2O_4Cl_2$ with pure five-coordinated pyramidal ligands were grown for the first time using a self-flux method, and the physical properties of these crystals were investigated. $Ca_3Cu_2O_4Cl_2$ is an antiferromagnetic Mott insulator with a Neel temperature of approximately 230 K. This material can be taken as an ideal parent structure of double $[CuO_2]$ layer high T_c cuprate superconductors. The unoccupied electronic structure of $Ca_3Cu_2O_4Cl_2$ was studied using polarization-dependent X-ray absorption spectroscopy. It was found that, unlike common high T_c cuprate superconductors, the UHB in $Ca_3Cu_2O_4Cl_2$ is a dominant spectral feature and well separated from the edge jump at the O *K*-edge. The anisotropic distribution of its holes is very similar to "214" high T_c cuprate. UHB is predominantly from the in-plane O $2p_x$, O $2p_y$, and Cu $3d_{x^2-y^2}$ orbitals, and the out-of-plane Cu $3d_{3z^2-r^2}$ orbitals are nearly fully occupied due to the lower energy level of $3d_{3z^2-r^2}$ in a five-coordinated pyramidal ligand.

Supporting Information

The supporting information is available online at phys.scichina.com and http://link.springer.com/journal/11433. The supporting materials are published as submitted, without typesetting or editing. The responsibility for scientific accuracy and content remains entirely with the authors.

This work was supported by the National Natural Science Foundation of China (Grant No. 11820101003), and the Ministry of Science & Technology (Grant Nos. 2018YFA0305701, 2017YFA0302901, and 2016YFA0300301).

1 J. G. Bednorz, and K. A. Müller, Z. Phys. B - Condens. Mat. **64**, 189 (1986).
2 S. Uchida, *High Temperature Superconductivity: The Road to Higher Critical Temperature* (Springer, Tokyo, 2014), Vol. 213.
3 C. Q. Jin, X. J. Wu, P. Laffez, T. Tatsuki, T. Tamura, S. Adachi, H. Yamauchi, N. Koshizuka, and S. Tanaka, Nature **375**, 301 (1995).
4 C. Q. Jin, R. Puzniak, Z. X. Zhao, X. J. Wu, T. Tatsuski, T. Tamura, S. Adachi, K. Tanabe, H. Yamauchi, and S. Tanaka, Phys. Rev. B **61**, 778 (2000).
5 R. Yu, Q. Liu, S. Zhang, X. Wang, W. Han, and C. Jin, Physica C **478**, 29 (2012).
6 C. Ye, P. Cai, R. Yu, X. Zhou, W. Ruan, Q. Liu, C. Jin, and Y. Wang, Nat. Commun. **4**, 1365 (2013), arXiv: 1201.0342.
7 C. Hu, J. F. Zhao, Y. Ding, J. Liu, Q. Gao, L. Zhao, G. D. Liu, L. Yu, C. Q. Jin, C. T. Chen, Z. Y. Xu, and X. J. Zhou, Chin. Phys. Lett. **35**, 067403 (2018), arXiv: 1805.10991.
8 W. Ruan, C. Hu, J. Zhao, P. Cai, Y. Peng, C. Ye, R. Yu, X. Li, Z. Hao, C. Jin, X. Zhou, Z. Y. Weng, and Y. Wang, Sci. Bull. **61**, 1826 (2016).
9 S. Feng, Phys. Rev. B **68**, 184501 (2003).
10 C. T. Chen, L. H. Tjeng, J. Kwo, H. L. Kao, P. Rudolf, F. Sette, and R. M. Fleming, Phys. Rev. Lett. **68**, 2543 (1992).
11 W. M. Li, L. P. Cao, J. F. Zhao, X. C. Wang, R. Z. Yu, Y. W. Long, Q. Q. Liu, and C. Q. Jin, Sci. China-Phys. Mech. Astron. **62**, 037421 (2018).
12 H. J. Lin, Y. Y. Chin, Z. Hu, G. J. Shu, F. C. Chou, H. Ohta, K. Yoshimura, S. Hébert, A. Maignan, A. Tanaka, L. H. Tjeng, and C. T. Chen, Phys. Rev. B **81**, 115138 (2010).
13 L. Tröger, D. Arvanitis, K. Baberschke, H. Michaelis, U. Grimm, and E. Zschech, Phys. Rev. B **46**, 3283 (1992).
14 C. Q. Jin, MRS Adv. **2**, 2587 (2017).
15 J. F. Zhao, W. M. Li, and C. Q. Jin, Sci. Sin.-Phys. Mech. Astron. **48**, 087405 (2018).
16 D. Vaknin, S. K. Sinha, C. Stassis, L. L. Miller, and D. C. Johnston, Phys. Rev. B **41**, 1926 (1990).
17 S. Haffner, R. Neudert, M. Kielwein, M. Knupfer, M. S. Golden, K. Ruck, G. Krabbes, J. Fink, H. Rosner, R. Hayn, H. Eisaki, S. Uchida, Z. Hu, M. Domke, and G. Kaindl, Phys. Rev. B **57**, 3672 (1998).
18 C. T. Chen, F. Sette, Y. Ma, M. S. Hybertsen, E. B. Stechel, W. M. C. Foulkes, M. Schulter, S. W. Cheong, A. S. Cooper, L. W. Rupp Jr., B. Batlogg, Y. L. Soo, Z. H. Ming, A. Krol, and Y. H. Kao, Phys. Rev. Lett. **66**, 104 (1991).